J Nanostruct 16(2): 1978-1989, Spring 2026

RESEARCH PAPER

A New Method for Enhancement Efficiency of Dye-Sensitized Solar Cells Based on TiO_2 Doped Ag Nanostructures as Photo-Anode

Wafaa Mahdi Salih [1], Osama Abdul Azeez Dakhil [1], Safanah Sahib Jaafar [2], Ahmed Mahdi Rheima [2]*

[1] *Physics Department, College of Science, Mustansiriyah University, Baghdad, Iraq*

[2] *Chemistry Department, College of Science, Mustansiriyah University, Baghdad, Iraq*

ARTICLE INFO

Article History:
Received 09 December 2025
Accepted 19 March 2026
Published 01 April 2025

Keywords:
Dye-sensitized solar cells
N719 dye
Sol-gel
TiO_2 doped Ag nanoparticles

ABSTRACT

Pure and silver-doped TiO_2 nanoparticles were synthesized using a unique and sustainable photo-irradiation method, in which red cabbage extract was used as an eco-friendly sensitizer. Ag dopants with different concentrations were prepared using the precursor materials technique. Red cabbage extract was introduced as the sensitizer dye. In the DSSCs, thin films of Ag-doped TiO_2 were employed as photo-anodes, and significant improvements in light-to-energy conversion efficiency were observed. The parameters of the DSSCs were measured, with the Ag-doped TiO_2 (0.03 mol) achieving the highest results, with a short-circuit current density (Jsc) of 10mA cm^{-2}, an open-circuit voltage of 0.8 V, filling factor of 39.37, and an overall energy conversion efficiency (η) of 3.15. As a result, when comparing the DSSCs with an undoped TiO_2 photo-anode, the power conversion efficiency of the Ag-doped TiO_2 cell increased significantly by 30% and 50% for the 0.01 and 0.03 mol concentrations, respectively.

How to cite this article
Salih W., Dakhil O., Jaafar S., Rheima A. A New Method for Enhancement Efficiency of Dye-Sensitized Solar Cells Based on TiO_2 Doped Ag Nanostructures as Photo-Anode. J Nanostruct, 2026; 16(2):1978-1989. DOI: 10.22052/JNS.2026.02.045

INTRODUCTION

Due to its comparatively high energy conversion efficiency and low cost, (DSSCs) have emerged as a viable substitutional to traditional solar cell-based silicon [1–3]. Semiconductors (TiO_2, NiO, ZnO, SnO_2, and $SrTiO_3$ have been widely investigated for photo-anode materials application in developing high-performance [4–8]. Because of its nontoxicity, chemical stability, premium electrical characteristics, and low cost, these structures are considered important semiconductors for various applications, including degradation, hydrogen production, photocatalysis, biosensors, and solar cells [9–12].

TiO_2 has been heavily doped with Pt, Au, Ag, and Cu to increase its characteristics. The dopant ions help to modify the electrical structure and absorb light in the TiO_2 layer. Noble metals, such as gold and silver, have electron-storing capabilities, allowing the separation of charges in semiconductor-metal composites [13,14].

Many studies have used Ag-doped TiO_2 as a photo-anode for DSSC applications, as it is inexpensive and the Ag work function is larger than the Fermi level of TiO_2, allowing for band gap efficient adjustment. Chang et al. [15] demonstrated that an Ag at TiO_2 photo-anode generates a permeable construction with not only a large surface area but also effective dye adsorption, and that a DSSC using such a photo-

* *Corresponding Author Email: dr.osama@uomustansiriyah.edu.iq*

anode obtained an efficiency of photoelectric conversion of 6.06 percent with a regulated film thickness. Using composite films made of Ag nanowires and TiO_2 nanoparticles, Huang et al. [16] demonstrated better electrons that transition between two surface transport and light harvesting in dye-sensitized solar cells. The DSSC's energy conversion efficiency with Ag NWs was 5.31 percent, whereas the DSSC without Ag NWs was 4.68 percent. Zohreh et al. [17] listed the efficiency at 6.51 percent with TiO_2:AgNP, reflecting a 27 percent efficiency increase for Ag NPs, and attributed it to the presence of Ag nanoparticles decreasing the energy band gap of TiO_2. Similar observations have been attributed by Gupta et al [18]. TiO_2 thin-film conductivity has risen photo-anode, resulting in the transport of fast electrons; as a result, the photocurrent has increased. L.S. Chougala1[19]. This study clarified the effect of the thickness of the photoanode on the efficiency of the solar cell, as its value varied from [5.4-8.6] using two types of dye [RK, N719] respectively.

The addition of Ag nanoparticles increases the interfacial charge-transfer mechanism while also encouraging charge separation within the TiO_2 coating. As a result, electrical conductivity improves [20]. In reality, diffusion dominates electron transport in DSSCs, and quicker electron transport leads to a greater photocurrent. The Ag-doped DSSC has a nearly threefold higher electron diffusion coefficient than the undoped DSSC, according to Li et al. [21]. Furthermore, silver dopants on TiO_2 might be blamed for speeding up the creation of the superoxide radical anion O^{2-} and reducing the likelihood of electron and hole recombination by scavenging electrons in the conduction band. It's possible that doping TiO_2 with silver ions (Ag^+ and Ag^{2+}) will produce a space charge to develop, with the e-/h couples separated effectively by the enormous electric field before recombination [20]. Furthermore, because silver's work function is bigger than TiO_2's Fermi level when they come into contact, a Schottky barrier is formed, which enhances the transport of TiO_2 photo-generated electrons to Ag NPs while delaying electron-hole pair recombination [22]. Another advantage of Ag/TiO_2 composites is that the spectrum of light absorption has been broadened. in the visible range due to Ag serving as the TiO_2 band gap electron traps [23].

This work employs a modified sol-gel technique with Urea as a capping agent [24-26] to synthesize undoped and Ag-doped TiO_2 (0.01, 0.03 mol), which is used to fabricate DSSCs. Many studies on Ag-doped TiO_2 for DSSCs have widely used different preparation techniques and chemical dyes such as N719 or Ruthenizer 535-bisTBA [27]. In contrast, this work uses red cabbage dye to offer a sustainable alternative with lower costs and environmental impact. Ongoing research aims to enhance the efficiency of natural dyes to make them more competitive with commercial options. The main goal is to improve the DSSC Performance by combining the effects of the capping agent and the dopant; significant augmentation of the sensitized photocurrent could be achieved.

MATERIALS AND METHODS

Materials

Titanium tetraisopropoxide ($[Ti(OCH(CH_3)_2)]_4$; 98%, Sigma-Aldrich), isopropanol ($(CH_3)_2CHOH$; 99.7%, Sigma-Aldrich), glacial acetic acid, urea (NH_2CONH_2; solid, 99%, Sigma-Aldrich) and silver nitrate ($AgNO_3$) were used as precursor materials for synthesis of TiO_2-doped Ag nanostructures. Silver was used to construct the counter electrodes. Potassium iodide (KI; solid, 98%, B.D.H) and iodine (I_2; solid, 99.9%, B.D.H) were added as a redox couple in the cell electrolyte. Red cabbage dye was used as a photosensitiser.

Irradiation cell

The irradiation cell consists of a medium-pressure mercury lamp with a source power of 125 watts and a maximum wavelength of 365 nm, as shown in Fig. 1. This cell contains a quartz tube that holds the ultraviolet source (i.e., the mercury lamp) and is in the form of a plunger in a tubular reactor made of Pyrex glass. The irradiation cell works as a reaction vessel for the chemical reaction, controlling the reaction parameters such as light intensity, wavelength, and exposure time of the precursor solution to light. Hence affects the nano products' properties.

Synthesis of TiO_2 Nanoparticles

Titanium tetraisopropoxide was used as a precursor material, with 30 ml added dropwise into a mixed solution of 15 ml isopropanol and 18 ml deionised water. To adjust the pH to the range of 7–8, 1.5 ml of glacial acetic acid diluted with 250 ml of deionised water was added to the above solution, and 4M urea was added dropwise

to prevent agglomeration. The mixture was placed inside a Pyrex tube and irradiated for half an hour using an ice bath. Following this exposure, the metal oxide solution was sonicated for one hour to avoid aggregation. A white precipitate was obtained, and to eliminate any particulates, the solution was filtered and the precipitate was then washed several times with distilled water and dried in an oven at 80 ºC for 12 hours. Calcination for two hours at 400 ºC was then performed to remove residual organics and stabilise the roducts. Fig. 2 illustrates a schematic diagram of preparing pure and doped TiO_2 NPs

Synthesis of Ag-doped TiO_2 Nanoparticles

Silver nitrate was dissolved in deionised water and then added dropwise to the above solution (titanium tetraisopropoxide–isopropanol) to obtain concentrations of 0.01 and 0.03 mol. Dilute nitric acid was then added until a pH value of 7–8 was achieved. To prepare the 0.01 and 0.03 mol Ag-doped TiO_2 samples, 6.76 mg and 20.28 mg masses of silver nitrate were used, respectively. A brownish-white precipitate was obtained. The

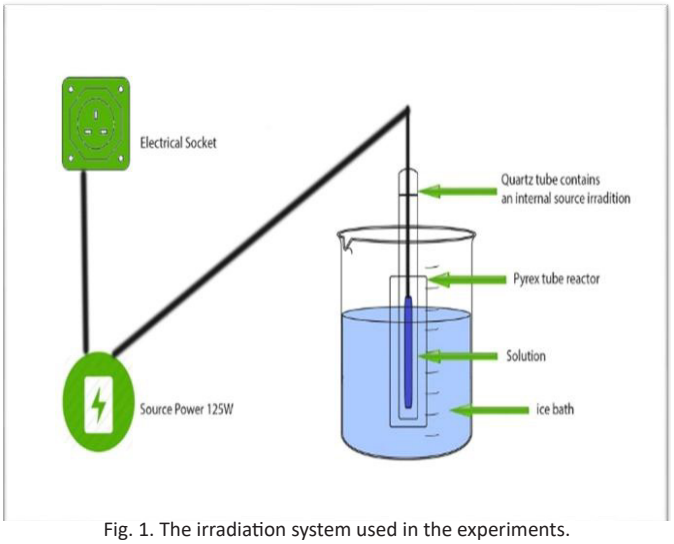

Fig. 1. The irradiation system used in the experiments.

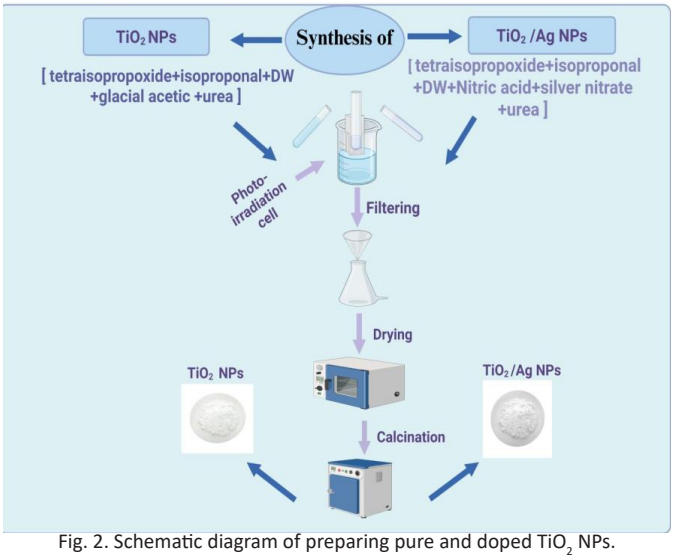

Fig. 2. Schematic diagram of preparing pure and doped TiO_2 NPs.

precipitates were filtered and rinsed multiple times with distilled water and ethanol to eliminate the nitrates. The dried sample was finally calcined at 400 ºC to obtain Ag-doped TiO_2 samples.

The pure TiO_2 sample was named S1, whereas the doped 0.01 and 0.03 mol samples were named S2 and S3, respectively.

Preparation of Dye from red cabbage (Brassica oleracea)

A mass of 100 g of fresh red cabbage was washed carefully using water and chopped into fine pieces approximately 1–2 cm in size, which were then heated in 200 mL of distilled water at 80 ºC for 30 minutes. Subsequently, the mixture was filtered through Whatman filter paper and then centrifuged at 2000 rpm for 15 minutes to remove any remaining debris. The red cabbage was stored at 20 ºC for later usage as a dye in the solar cells. The use of this dye, compared to other organic dyes [28], yielded better results in terms of efficiency.

The effectiveness of red cabbage as a dye for DSSCs – both in terms of its chemical composition and the resulting FTIR spectra – is essential. Red cabbage contains various compounds that contribute to its colour and potential as a dye, including anthocyanins. The presence of anthocyanins suggests good light absorption in the visible spectrum, particularly in the blue–green region. Red cabbage also contains flavonoids and phenolic compounds, which provide additional colour stability and antioxidant activity. The FTIR spectrum of red cabbage dye, as shown in Fig. 3, exhibits characteristic peaks corresponding to various functional groups: O-H stretching (broad peak around 3200–3600 cm^{-1}, indicating the presence of hydroxyl groups in anthocyanins and flavonoids), C=C stretching (peaks around 1500–1600 cm^{-1}, associated with the aromatic rings of the flavonoids), and C-O stretching (peaks around 1000–1300 cm^{-1}, indicating the presence of glyosidic bonds in anthocyanins).

Fabrication of DSSC

To fabricate the DSSC, a glass substrate covered with FTO was first cut into 2×2 cm pieces, which were then rinsed with ethanol, followed by deionized water, and dried. TiO_2 and TiO_2-doped Ag were deposited on the substrate using the doctor's blade method. The thermal evaporation technique model was used to evaporate Ag onto the back contact using a grid mask. Using the doctor's blade process, TiO_2 and TiO_2 doped with different concentrations of Ag nanopowder (0.01 and 0.03 mol) were coated onto a surface area of 0.2 cm^2 of the FTO. TiO_2 and TiO_2/Ag nanopowders were combined with a small amount of Triton-X 100, acetylacetone, and ultrapure water in a pestle to prepare a paste for the coating. A razor blade was used to deposit the paste onto the FTO surface to form TiO_2 or TiO_2/Ag coatings. The resulting film was annealed at 150 ºC for 1 hour to eliminate organic residues. The annealed film was soaked in red cabbage dye solution in the dark for two hours at room temperature. The resulting photo-anode was red–grey. The dye-absorbed TiO_2 and TiO_2/Ag films were then clipped with

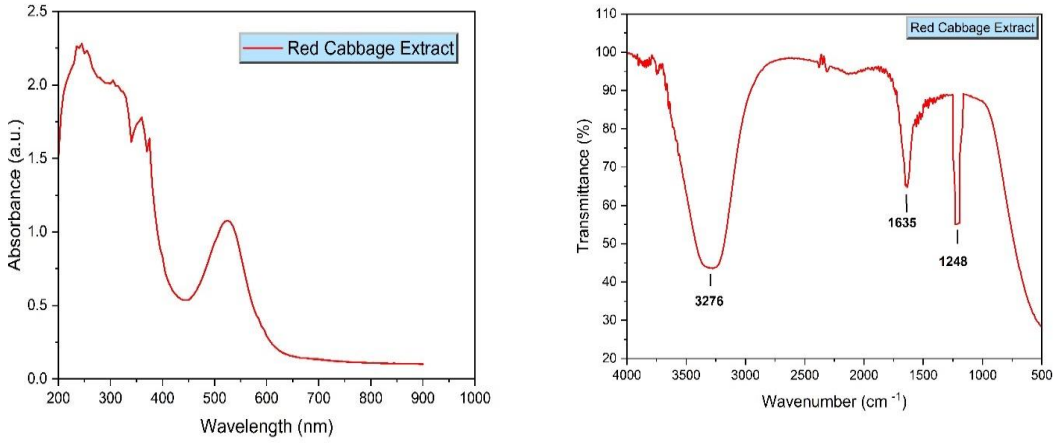

Fig. 3. Absorbance and FTIR of red cabbage extract.

aluminum-coated counter electrodes to generate sandwich-type DSSC structures. For the last stage of DSSC production, the redox electrolyte (0.2 M lithium iodide and 0.02 M iodine in propylene carbonate) was pumped into the device through the gap in the counter electrode.

Characterization of TiO_2 and Ag-doped TiO_2 nanoparticles

Using CuKα radiation (λ=1.54056), an XRD analyzer (Philips PW1730) was used to determine the phases contained in the synthesized TiO_2 and Ag-doped TiO_2 nanoparticles within a 2Θ range of 20–80º. The morphology of the TiO_2 and Ag-TiO_2 nanoparticles was studied using FESEM (ZEISS) and TEM (ZEISS), while EDX analysis was used to determine their elemental composition. The absorption spectra were calculated using a SHIMADZU UV-3600 Plus spectrophotometer. In addition, the photocurrent-voltage properties of the TiO_2 and TiO_2/Ag DSSCs were investigated using a variable resistor box and two Avometers, one of which was connected in parallel with the fabricated solar cell to measure voltages and the other was connected in series to measure the current. This apparatus was used on a solar simulator to collect measurements in the presence of lighting with an AM1.5 power density (100 mW/

Table 1. Crystal size, FWHM, 2Θ, Micro strain, and dislocation density.

Samples	Crystallite size for highest peak (nm)	FWHM (degree)	2Θ	d-spacing (Aº)	Strain (10^{-4})	Dislocation density(10^{-3}) (line/nm^2)
S1	10.83	0.7872	25.3	3.50876	85.2	17.18
S2	9.84	0. 8720	25.3	3.51675	103.2	18.08
S3	8.72	0.9840	25.3	3.51693	131.5	19.19

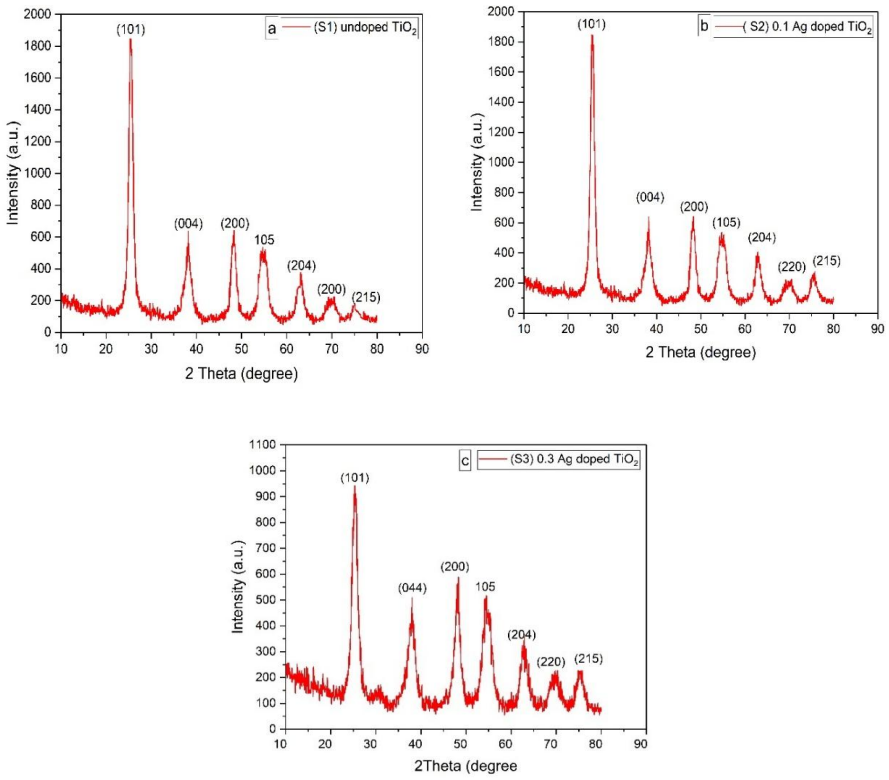

Fig. 4. XRD spectra for (a) S1 (b) S2, and (c) S3.

cm^2).

RESULTS AND DISCUSSION

Structural properties of TiO_2 and Ag-doped TiO_2 nanoparticles

X-ray powder diffraction patterns for S1, S2, and S3 are depicted in Fig. 4a-c, respectively. The diffraction peaks observed at 2Θ=25.3, 37.9, 48.1, 54.9, and 62.7 correspond to the (101), (004), (200), (211), and (204) planes, respectively. These observations confirm the formation of the anatase phase of TiO_2 and Ag-doped TiO_2 only without the presence of the rutile phase. All the experimental XRD spectra were matched with JCPDS PDF No. 021-44862778. The diffraction peaks of the synthesized TiO_2 and Ag-doped TiO_2 nanoparticles were broadened due to their preserved nanostructure even after calcination. Peak broadening can also be caused by severe strain, instrument errors, and other factors [29-32]. We used Scherer's equation [33] to compute the crystallite size of the prepared TiO_2 and TiO_2-doped Ag nanoparticles.

$$G.z=k\lambda/\beta \cos\Theta \quad (1)$$

Where k is a constant equal to 0.89, λ is the CuKα wavelength (1.5418 Aº), β is the full-width half maximum (FWHM) of the peak (radians), and Θ is the diffraction angle (degrees).

For the strongest peak at 25.3º (101), the crystal sizes for the TiO_2 powder were determined as 10.83nm (S1), 12.92nm (S2), and 9.84nm (S3). The average crystallite sizes of the samples calculated using the diffraction peaks for the (101), (004), (200), (211), and (204) planes were 15.7 nm (S1), 15.6 nm (S2), and 22.9 nm (S3). The Ag-doped TiO_2 samples' XRD patterns are nearly identical to those of pure TiO_2, with no diffraction peaks attributable to the silver species, implying that the metal particles are well disseminated across the TiO_2 surface. The crystal structure of the anatase TiO_2 is unaffected by Ag doping, indicating that the metal dopant is simply situated on the crystal's surface rather than being covalently attached to the crystal lattice. In the XRD patterns, there are

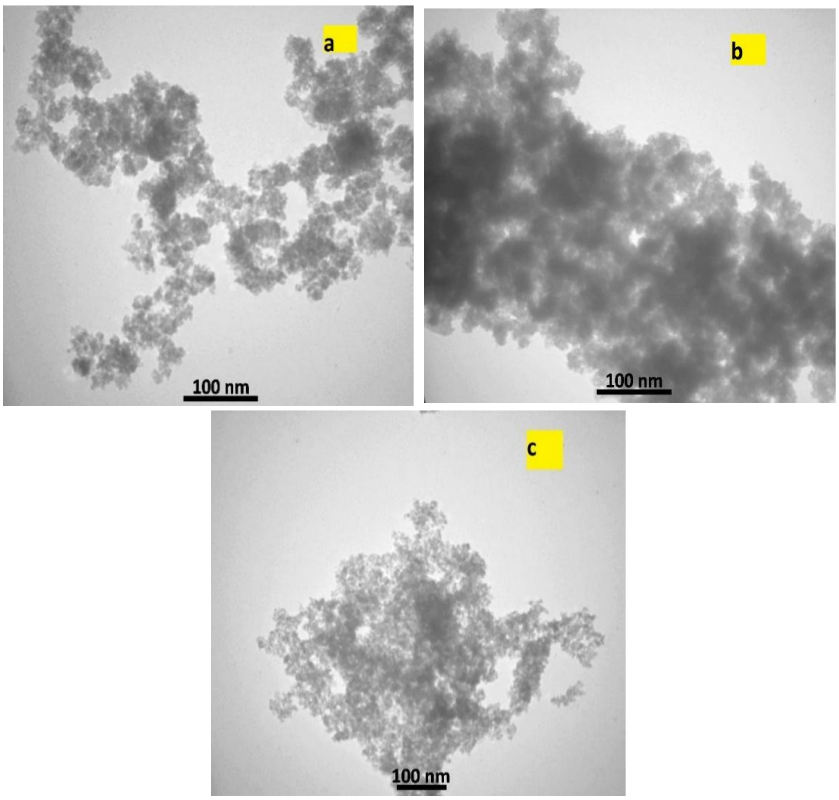

Fig. 5. TEM images of (a) S1, (b) S2, and (c) S3.

no diffraction pattern features corresponding to Ag metal.

Morphological analysis of TiO_2 and Ag-doped TiO_2 nanoparticles

The sizes and morphologies of the synthesised nanoparticles were determined using the TEM technique. The presence of Ag in the Ag-doped TiO_2 particles is nearly confirmed by TEM characterization. As demonstrated in Fig. 5, samples S1, S2, and S3 had average particle diameters of 8–12 nm, 2–6 nm, and 4–7 nm, respectively. Smaller TiO_2 particles have a larger surface area and more joint sites between colloidal particles at the particle–core substrate interface, allowing for improved dye adsorption[34]. Additionally, TiO_2 nanoparticles with sizes less than 10 nm consist of a lattice of modulated-diameter TiO_2 nanoparticles

Table 2. Practical EDX data.

Samples	Element	Line type	Weight%	Atomic %
S1	O	K series	47.15	72.76
	Ti	K series	52.85	27.24
	Ag	-	-	-
	total		100.00	100.00
S2	O	K series	48.24	73.96
	Ti	K series	50.14	25.67
	Ag	Lseries	1.62	0.37
	total		100.00	100.00
S3	O	K series	50.15	75.52
	Ti	K series	47.73	24.01
	Ag	Lseries	2.12	0.47
	total		100	100

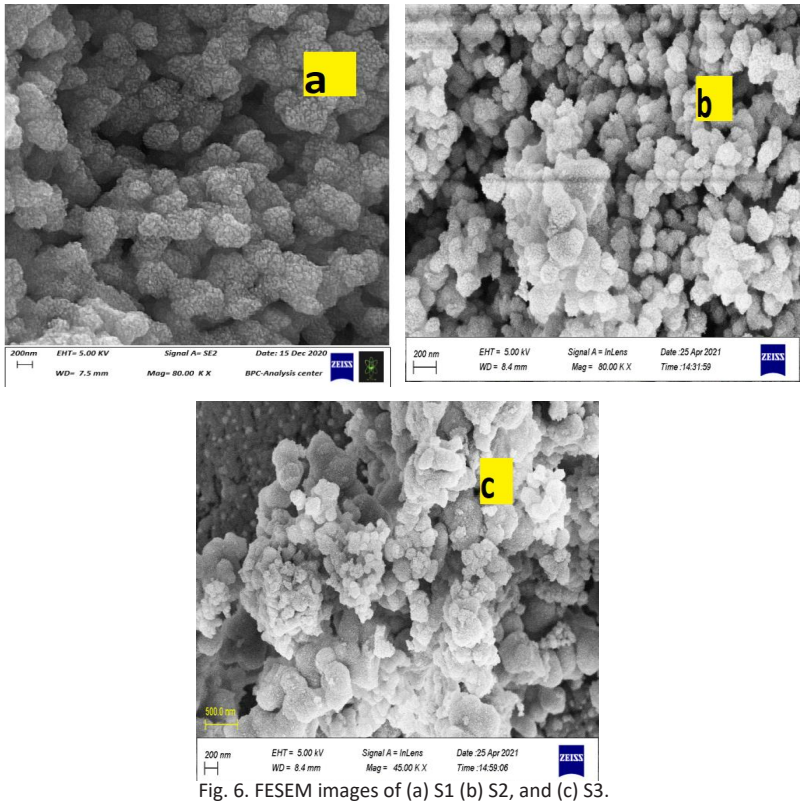

Fig. 6. FESEM images of (a) S1 (b) S2, and (c) S3.

and interstitial regions filled with electrolyte. This configuration not only enhances light trapping and absorption but also offers improved electrical transport through the nanoTiO_2 particles [28]. In both the Ag-doped samples, the particles are irregular in form but exhibit agglomeration.

The morphology of samples S1, S2, and S3 is shown in Fig. 6 a-c, respectively. The spherical nature of the synthesized nanoparticles with identical diameters is depicted in the FESEM microstructure. The spherical, undoped TiO_2 nanoparticles were found to have an average size of about 40 nm. Because of their small size, the TiO_2 nanoparticles are homogeneous with negligible aggregation. To reduce agglomeration, we used urea, which is a cost-efficient capping chemical. Although samples S2 and S3 exhibit clusters of agglomerated nanoparticles with diameters of roughly 30 nm, this is a good result compared to [35]. The presence of a complex, porous, sponge-like structure is confirmed by the FESEM images of the Ag-doped TiO_2 nanoparticles. Such a structure implies a large surface area, thus resulting in increased dye adsorption, which is effective in DSSC applications. The penetration of the electrolyte is aided by the presence of this structure, which is interpreted to improve efficiency. The distribution of Ag on the surface of the TiO_2 is non-uniform, with a significant amount of Ag present in the Ag-doped TiO_2. Irregularly shaped particles are observed that result from the aggregation of small crystals. Fig. 7 Shows the EDX spectra used to investigate the elemental composition of the TiO_2 and Ag-doped TiO_2 nanoparticles, and Table 2 shows the experimentally determined atomic percentages of Ti, O, and Ag.

Electrical characterization of TiO_2 and Ag-doped TiO_2 nanoparticles as photo-anodes

Both doped and undoped TiO_2 nanoparticles

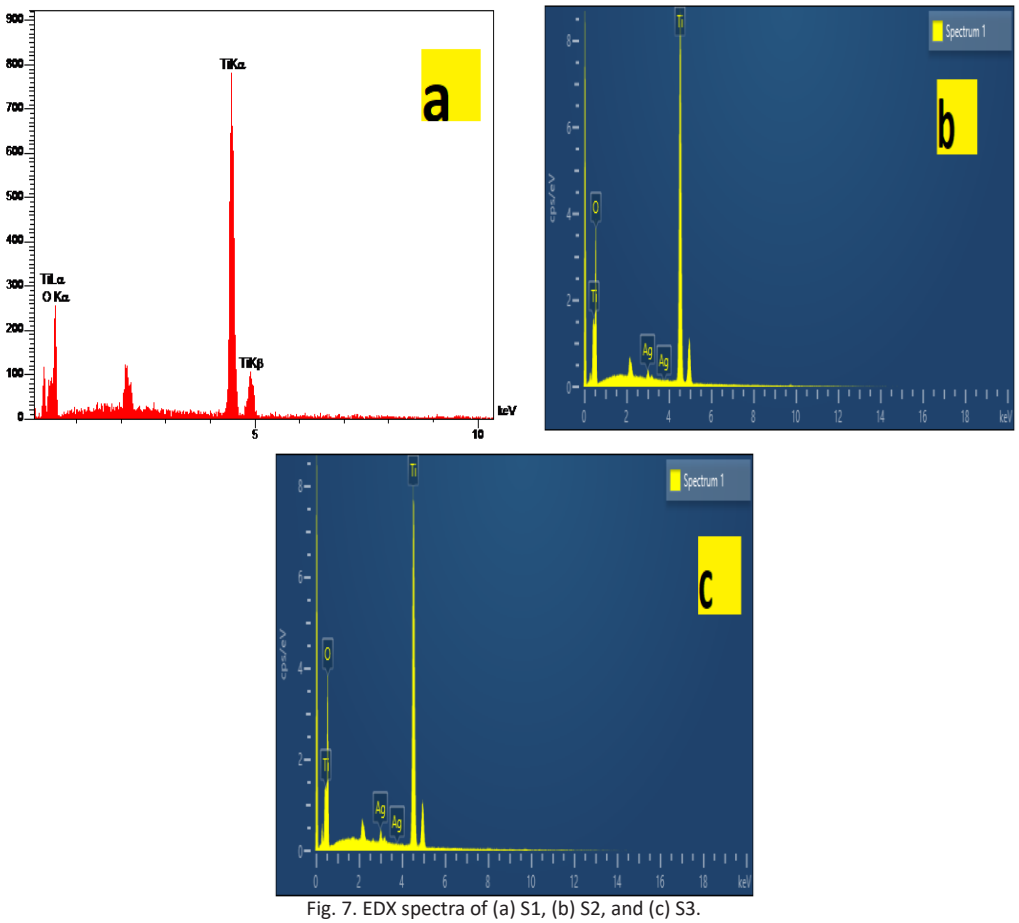

Fig. 7. EDX spectra of (a) S1, (b) S2, and (c) S3.

were used to construct photo-anodes, which were then used to fabricate DSSCs after being immersed in red cabbage dye. The photocurrent–potential (J–V) curves of these cells are shown in Fig. 8 for illuminations of less than 100 mW/cm^2. The following relationships were used to evaluate the power conversion efficiency (η) and fill factors (F.F.) based on the J–V curves:

$$\eta = \frac{Pm}{Pin} * 100\% \quad (2)$$

$$\eta = \frac{F.F\ IscVoc}{Pin} * 100\% \quad (3)$$

$$F.F = \frac{ImVm}{IscVoc} \quad (4)$$

The electron lifetime (τ) can be estimated from the open-circuit voltage (Voc) and other parameters using the following relationship:

$$\tau = \frac{n * kt}{q * I_O} \quad (5)$$

Where, τ: Electron life time, n: Electron density, kt: conductivity constant =q·μ·n

q: the electron charge 1.6*10^{-19}, and Io: output current.

Whereas Voc, Jsc, and Iinc represent the open-circuit potential, short-circuit photocurrent, and incident light intensity, respectively. The efficiency and fill factor values for undoped TiO_2 were 2.16% and 46.79, respectively, whereas, under similar conditions, the equivalent values for S2 were 2.76% and 48.08, while those for S3 were 3.15% and 39.37, respectively. Table 3 summarises these output parameters. As a result, the photocurrent values of the solar cells constructed with 0.01 mol and 0.03 mol Ag-doped TiO_2 electrodes increased by 30% and 50% relative to undoped TiO_2. In addition, an electron lifetime value of 1.24 ms was recorded for undoped TiO_2, which increased to 2.43 and 3.28 ms in S2 and S3, respectively. This result is comparable with those of [35] and [36] and outperforms [34]. The Voc values of the DSSCs with 0.01 and 0.03 mol Ag-doped TiO_2 electrodes also increased.

Ag doping in TiO_2 plays a multifaceted role in enhancing the performance of DSSCs. By reducing the bandgap [36-40], Ag doping introduces new energy levels within the bandgap of TiO_2. These levels are attributed to the presence of Ag ions and

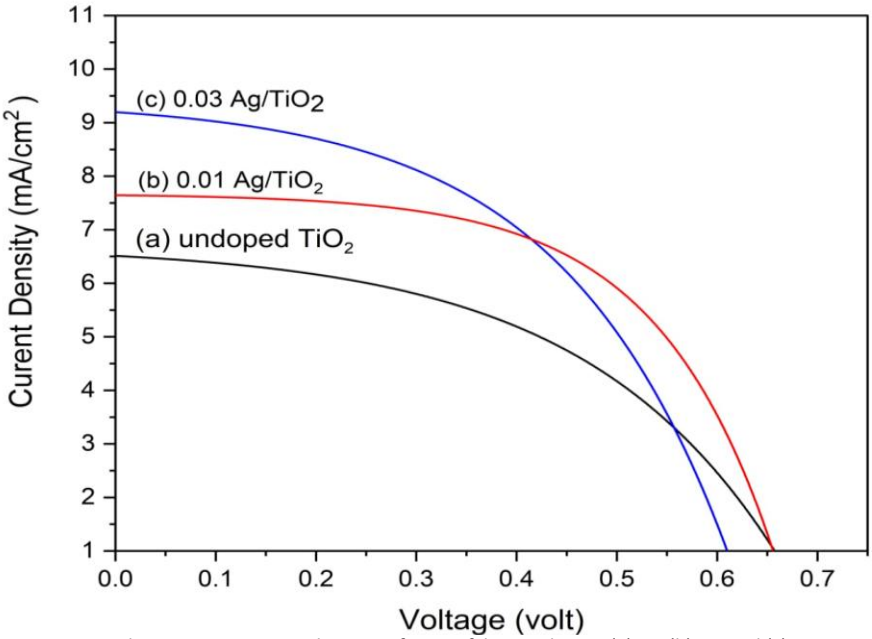

Fig. 8. Photocurrent–potential curves of DSSCs fabricated using (a) S1, (b) S2, and (c) S3.

Table 3. The photovoltaic parameters of undoped TiO_2 and Ag-doped TiO_2 DSSCs.

Samples	J_{sc}(Ma/cm^2)	V_{oc} (volt)	ɳ (%)	F.F. (%)
S1	7.0	0.65	2.16	46.79
S2	8.2	0.70	2.76	48.08
S3	10	0.80	3.15	39.37

their interactions with the TiO_2 lattice. Introducing these mid-gap states can facilitate the excitation of electrons at lower energy levels, effectively narrowing the bandgap. By improving electron transport, Ag ions can act as electron traps that prolong the lifetime of excited electrons. This phenomenon is crucial because longer electron lifetimes can lead to higher photocurrent values and minimise recombination processes, thus significantly increasing the efficiency and stability of solar cells. Continued research into optimal doping concentrations and methods can further maximise these benefits, making Ag-doped TiO_2 a promising area of study in solar energy applications [41-43].

The electron lifetime in S1 was increased from 1.24 ms to 2.43 and 3.28 ms in S2 and S3, respectively, reducing electron recombination. Thus, the enhanced Jsc values in DSSCs containing Ag-doped TiO_2 electrodes may relate to improved dye adsorption and longer electron lifetimes. The recorded increase in Jsc is primarily due to the increased optical absorption of incident photons. Because the Ag doping process increased Jsc, the resistance was reduced compared to undoped TiO_2. This may be because Ag nanoparticles shorten the electron transport paths in photoanodes, thereby improving electron transfer efficiency from the TiO_2 layer to the substrate.

In comparison to previously published studies with similar TiO_2 nanoparticle architectures [44], the efficiency of the manufactured TiO_2-based DSSC in the present work was found to be acceptable. The dipping time of a TiO_2 film into a sensitizing dye has been revealed to be a crucial element for determining the solar cell characteristics of the resulting TiO_2-based DSSC [16]. In comparison to similar research [18], the manufactured TiO_2-based DSSC in this study exhibited superior efficiency after a shorter dipping duration.

Increased absorption due to an increase in the number of dye molecules adsorbed onto the TiO_2 surface may also explain the high efficiency of the synthesised materials. Because the procedure is straightforward and the samples are simple to create, the use of TiO_2 nanoparticles in photovoltaic applications has a promising future. The present density value was found to be quite low. The photocurrent is the most significant parameter that defines the system's overall efficiency limit. Due to their high surface area and surface energy, the parent materials react differently as their particle sizes approach the nanoscale [45,46].

CONCLUSION

The fabrication of a photo-anode for DSSC applications was demonstrated using a photo-irradiation method, which was used to prepare TiO_2 and optimised Ag-doped TiO_2 nanoparticles, which were employed as photoelectrodes using the simple doctor's blade method. The generated TiO_2 samples were mostly composed of the anatase phase of titanium based on XRD analysis. This work introduced the use of organic dyes instead of polluting chemical dyes and succeeded in increasing the efficiency of the obtained DSSCs. The use of Ag as a dopant successfully reduced and red-shifted the material's optical band gap, with corresponding changes in its ability to absorb visible light. In Ag-doped TiO_2, the electron lifetime of DSSC increased from 1.27 ms to 2.4 and 3.28 ms for 0.01 and 0.03 mol Ag concentrations, respectively, when compared to undoped TiO_2. Compared to the pure TiO_2 photo-anode-based DSSC, the device produced utilising Ag-doped TiO_2 had better Jsc values due to the longer ɾn. Based on sample characterisation, the improved Jsc and ɳ values and better photovoltaic performance were attributed to the surface saturation of the Ag-doped TiO_2 with sensitising dye.

ACKNOWLEDGMENTS

The authors would like to thank Mustansiriyah University (www. www.uomustansiriyah.edu.iq)

Baghdad, Iraq, for its support in the present work.

CONFLICT OF INTEREST

The authors declare that there is no conflict of interests regarding the publication of this manuscript.

REFERENCES

1. O'Regan BC, Durrant JR. Kinetic and Energetic Paradigms for Dye-Sensitized Solar Cells: Moving from the Ideal to the Real. Acc Chem Res. 2009;42(11):1799-1808.
2. Wei D. Dye Sensitized Solar Cells. Int J Mol Sci. 2010;11(3):1103-1113.
3. Lv C, Wang X, Li Q, Li C, Ouyang Q, Liu Y, et al. Template-assisted synthesis of porous TiO2 photoanode for efficient dye-sensitized solar cells – CORRIGENDUM. J Mater Res. 2020:1-1.
4. Mohammed RQ, Ahmed BM. Performance enhancement of ZnO/Zn nanostructure biosensor via cold atmosphere plasma. J Nanopart Res. 2024;27(1).
5. Fujishima A, Rao TN, Tryk DA. Titanium dioxide photocatalysis. Journal of Photochemistry and Photobiology C: Photochemistry Reviews. 2000;1(1):1-21.
6. Yang S, Kou H, Wang H, Cheng K, Wang J. Preparation and Band Energetics of Transparent Nanostructured $SrTiO_3$ Film Electrodes. The Journal of Physical Chemistry C. 2009;114(2):815-819.
7. Lusvardi G, Barani C, Giubertoni F, Paganelli G. Synthesis and Characterization of TiO2 Nanoparticles for the Reduction of Water Pollutants. Materials. 2017;10(10):1208.
8. Hagfeldt A, Boschloo G, Sun L, Kloo L, Pettersson H. Dye-Sensitized Solar Cells. Chem Rev. 2010;110(11):6595-6663.
9. Mohammed RQ, Ahmed BM. Enhanced Nonenzymatic Glucose Biosensor of ZnO Nanostructure via Nonthermal Plasma. International Journal of Nanoscience. 2024;23(06).
10. Zaid HM, Fakhruldi H, Yow FY, Razali N, Dasan YK. Synthesis and Characterization of Titanium Dioxide Nanoparticles for Application in Enhanced Oil Recovery. Defect and Diffusion Forum. 2019;391:74-81.
11. Hu Y, Tsai HL, Huang CL. Effect of brookite phase on the anatase–rutile transition in titania nanoparticles. J Eur Ceram Soc. 2003;23(5):691-696.
12. Crişan D, Drăgan N, Răileanu M, Crişan M, Ianculescu A, Luca D, et al. Structural study of sol–gel Au/TiO2 films from nanopowders. Appl Surf Sci. 2011;257(9):4227-4231.
13. Liu Y, She G, Qi X, Mu L, Wang X, Shi W. Contributions of Ag Nanowires to the Photoelectric Conversion Efficiency Enhancement of TiO_2 Dye-Sensitized Solar Cells. Journal of Nanoscience and Nanotechnology. 2015;15(9):7068-7073.
14. Dissanayake MAKL, Kumari JMKW, Senadeera GKR, Thotawatthage CA. Efficiency enhancement in plasmonic dye-sensitized solar cells with TiO_2 photoanodes incorporating gold and silver nanoparticles. J Appl Electrochem. 2015;46(1):47-58.
15. Devadiga D, Selvakumar M, Shetty P, Mahesha MG, Devadiga D, Ahipa TN, et al. Novel photosensitizer for dye-sensitized solar cell based on ionic liquid–doped blend polymer electrolyte. J Solid State Electrochem. 2021;25(4):1461-1478.
16. Huang P-C, Chen T-Y, Wang Y-L, Wu C-Y, Lin T-L. Improving interfacial electron transfer and light harvesting in dye-sensitized solar cells by using Ag nanowire/ TiO_2 nanoparticle composite films. RSC Advances. 2015;5(86):70172-70177.
17. Mahmoudabadi ZD, Eslami E, Narimisa M. Synthesis of Ag/TiO_2 nanocomposite via plasma liquid interactions: Improved performance as photoanode in dye-sensitized solar cell. Journal of Colloid and Interface Science. 2018;529:538-546.
18. Gupta AK, Srivastava P, Bahadur L. Improved performance of Ag-doped TiO_2 synthesized by modified sol–gel method as photoanode of dye-sensitized solar cell. Appl Phys A. 2016;122(8).
19. Chougala LS, Yatnatti MS, Linganagoudar RK, Kadadevarmath JS. Synthesis and Characterization of ZnO Nanoparticles and Its Application to Dye Sensitized Solar Cell. Advanced Science Letters. 2018;24(8):5618-5623.
20. Hou X, Ma H, Liu F, Deng J, Ai Y, Zhao X, et al. Synthesis of Ag ion-implanted TiO_2 thin films for antibacterial application and photocatalytic performance. J Hazard Mater. 2015;299:59-66.
21. Li J, Chen X, Ai N, Hao J, Chen Q, Strauf S, et al. Silver nanoparticle doped TiO_2 nanofiber dye sensitized solar cells. Chem Phys Lett. 2011;514(1-3):141-145.
22. Prasher P, Sharma M. Synthesis of Silver Nanoparticles. Silver Nanoparticles: Synthesis, Functionalization And Applications: Bentham Science Publishers; 2022. p. 22-44. http://dx.doi.org/10.2174/9789815050530122010004
23. Gutiérrez DJR, Mathews NR, Martínez SS. Photocatalytic activity enhancement of TiO_2 thin films with silver doping under visible light. J Photochem Photobiol A: Chem. 2013;262:57-63.
24. Seo DS, Kim H, Jung HC, Lee JK. Synthesis and characterization of TiO_2 nanocrystalline powder prepared by homogeneous precipitation using urea. J Mater Res. 2003;18(3):571-577.
25. Favier L, Sescu AM, Abdelkader E, Oughebbi Berthou L, Lutic D. Urea-Assisted Synthesis of Mesoporous TiO_2 Photocatalysts for the Efficient Removal of Clofibric Acid from Water. Materials. 2021;14(20):6035.
26. Asif M, Zafar M, Akhter P, Hussain M, Umer A, Razzaq A, et al. Effect of Urea Addition on Anatase Phase Enrichment and Nitrogen Doping of TiO_2 for Photocatalytic Abatement of Methylene Blue. Applied Sciences. 2021;11(17):8264.
27. Ramadhani DAK, Sholeha N, Khusna NNa, Diantoro M, Afandi AN, Osman Z, et al. Ag-doped TiO_2 as photoanode for high performance dye sensitized solar cells. Materials Science for Energy Technologies. 2024;7:274-281.
28. Kumar Rout S, Padhi P, Biswal M, Debata S. A Comparative Study of a Novel Technique for the Fabrication of Dye Sensitized Solar Cells Using Nano TiO_2 and Different Dyes. Research & Reviews: Journal of Material Sciences. 2018;06(01).
29. Alhayani BSA, Ilhan H. Visual sensor intelligent module based image transmission in industrial manufacturing for monitoring and manipulation problems. J Intell Manuf. 2020;32(2):597-610.
30. Alhayani B, Abdallah AA. RETRACTED: Manufacturing intelligent Corvus corone module for a secured two way image transmission under WSN. Engineering Computations. 2020;38(4):1751-1788.
31. Rajendrachari S. Investigation of Electrochemical Pitting Corrosion by Linear Sweep Voltammetry: A Fast and Robust Approach. Voltammetry: IntechOpen; 2019.
32. Alhayani B, Kwekha-Rashid AS, Mahajan HB, Ilhan H, Uke N, Alkhayyat A, et al. 5G standards for the Industry 4.0 enabled communication systems using artificial intelligence: perspective of smart healthcare system. Applied Nanoscience. 2022;13(3):1807-1817.

33. Blessymol B, Kalaiselvi V, Yasotha P, Gopi S. Comparative Study of Chemically and Green Synthesized Titanium Dioxide Nanoparticles using Leucas aspera Leaf Extract. Journal of Environmental Nanotechnology. 2023;12(3):10-13.
34. Mahmoud SA, Mohamed BS, Killa HM. Synthesis of Different Sizes TiO_2 and Photovoltaic Performance in Dye-Sensitized Solar Cells. Frontiers in Materials. 2021;8.
35. Enhancing Efficiency in Dye-Sensitized Solar Cells: Incorporation of Cu_3VSe_4 Nanocrystals into TiO_2 Photoanodes. American Chemical Society (ACS).
36. Rathnasekara R, Hari P. Enhancing the Efficiency of Dye-Sensitized Solar Cells (DSSCs) by Nanostructured Ag-doped ZnO Electrodes. ChemistrySelect. 2022;7(29).
37. Rathod PB, Waghuley SA. Synthesis and UV-Vis spectroscopic study of TiO_2 nanoparticles. International Journal of Nanomanufacturing. 2015;11(3/4):185.
38. Tripathi TS, Terasaki I, Karppinen M. Anomalous thickness-dependent optical energy gap of ALD-grown ultra-thin CuO films. J Phys: Condens Matter. 2016;28(47):475801.
39. Usha K, Mondal B, Sengupta D, Das P, Mukherjee K, Kumbhakar P. Fabrication of Dye Sensitized Solar Cell Using Nanocrystalline TiO_2 and Optical Characterization of Photo-Anode. Nanoscience and Nanoengineering. 2014;2(2):29-35.
40. Munir S, Shah SM, Hussain H, Ali khan R. Effect of carrier concentration on the optical band gap of TiO2 nanoparticles. Materials & Design. 2016;92:64-72.
41. Chougala LS, Yatnatti MS, Linganagoudar RK, Kamble RR, Kadadevarmath JS. A Simple Approach on Synthesis of TiO_2 Nanoparticles and its Application in dye Sensitized Solar Cells. Journal of Nano- and Electronic Physics. 2017;9(4):04005-04001-04005-04006.
42. Dubey RS, Jadkar SR, Bhorde AB. Synthesis and Characterization of Various Doped TiO_2 Nanocrystals for Dye-Sensitized Solar Cells. ACS Omega. 2021;6(5):3470-3482.
43. He X, Guo Y, Li X, Liu J. In situ ligand-free growth of TiO_2-escapsulated Au nanocomposites on photoanode for efficient dye sensitized solar cells. Chem Eng J. 2020;396:125302.
44. Rajendrachari S, Debasis C, Dibyendu C. Fabrication of Nano-Yttria Dispersed Duplex and Ferritic Stainless Steels by Planetary Milling Followed by Spark Plasma Sintering and Non-Lubricated Sliding Wear Behaviour Study. Journal of Materials Science and Engineering B. 2016;6(3).
45. Abu-Rumman A. Transformational leadership and human capital within the disruptive business environment of academia. World Journal on Educational Technology: Current Issues. 2021;13(2):178-187.
46. Mahajan HB, Rashid AS, Junnarkar AA, Uke N, Deshpande SD, Futane PR, et al. Integration of Healthcare 4.0 and blockchain into secure cloud-based electronic health records systems. Applied Nanoscience. 2022;13(3):2329-2342.